Journal of Biomedical Optics 7(4), 643–649 (October 2002)

Analysis on performance and optimization of frequency-domain near-infrared instruments

Tao Tu
University of Pennsylvania
Department of Electrical Engineering
Department of Biochemistry and Biophysics
Philadelphia, Pennsylvania 19104

Yu Chen
University of Pennsylvania
Department of Bioengineering
Department of Biochemistry and Biophysics
Philadelphia, Pennsylvania 19104

Jun Zhang
Xavier Intes
Britton Chance
University of Pennsylvania
Department of Biochemistry and Biophysics
Philadelphia, Pennsylvania 19104

Abstract. Frequency-domain near-infrared techniques have been widely used to detect the optical properties of biological tissues noninvasively. In this paper we propose an analytical model to evaluate the performance of frequency-domain instruments. Based on the diffusion equation and the transfer properties of optoelectronic components, we treat all parts, including the medium, as two-port networks and apply systematic methods to answer questions concerning frequency-domain instruments. Experiments show that this method can reasonably reflect the properties of the instrument within an accuracy of 7%. This kind of method can be used to design suitable instruments for various applications. We also analyze the selection of the instrument parameters to achieve optimal performance at an efficient cost using this analytical model. [DOI: 10.1117/1.1501562]

Keywords: frequency domain; noninvasive near-infrared detection; photon diffusion; noise model; diffuse optical spectroscopy.

Paper JBO 01068 received Oct. 9, 2001; revised manuscript received May 8, 2002 and June 24, 2002; accepted for publication June 25, 2002.

1 Introduction

Noninvasive near-infrared (NIR) spectroscopy and imaging, which can be used to study the physiological state of biological tissues by detecting their optical properties, have long been investigated. Many techniques have been presented.[1–6] In these techniques, continuous wave (cw) instruments measure only light intensity, however frequency-domain (FD) and time-domain (TD) instruments utilize the additional phase or time information and are capable of quantitative measurements of the optical properties. Compared to TD instruments, which have better sensitivity, FD instruments are more economical and suitable for real time clinical usage. Theories of intensity modulated light diffusion in highly scattering media have been studied[7,8] and several kinds of FD instruments have been demonstrated to provide accurate results.[9–13]

However, there are still some unresolved questions about FD systems. We cannot not know its performance when we build an instrument. First, in a given circumstance such as brain imaging, how large a separation can the source-detector pair achieve? Generally, the larger the separation, the deeper the light that goes through the tissue and the more information we can obtain.[14] When we want to detect an object deep under the skin, the source–detector pair must have enough separation to give useful information. Second, how do the parameters of the instrument, such as laser power, diameter of the detecting fiber, high voltage of the photomultiplier tube (PMT), etc., affect its performance? What are the minimum requirements these parameters should fulfill in a specific application? Third, answers to the second question also give us guidance in optimizing the instrument and enhancing its performance at an efficient cost. All these questions require a thorough and systematic analysis of FD instruments.

Address all correspondence to Tao Tu. Tel: 215-898-4387; Fax: 215-898-1806; E-mail: tutao@mail.med.upenn.edu

In this paper, we present a transmission model of the radio frequency (rf) signal in the FD instrument based on diffusion theory and the transfer properties of the optoelectronic components. We will then give a detailed analysis of its performance and the factors influencing it. Experiments have also been performed to verify our analysis.

2 Basic Theory

2.1 Transmission Model of the rf Signal

The purpose of FD instruments is to detect the amplitude and phase changes of the rf signal after it passes through a turbid medium on the optical carrier. That means the optical link from the source to the detector is a basic part of the instrument. Other electronic parts, such as amplifiers, band pass filters, *IQ* demodulators, low pass filters, etc., act as ''a special filter'' and help to pick up the rf signal to measure its amplitude and phase. Then the transmission process in FD instruments can be outlined as shown in Figure 1. It is similar to the subcarrier multiplexed (SCM) system in fiber optical communication fields.[15,16] The rf signal is added to the light in the laser diode (LD), and it then passes through the source fiber, medium and detecting fiber, and is at last received and recovered by the optical detector (the PMT is used in Figure 1).

Each component in Figure 1, including the medium, can be treated as a network with two ports (an in port and an out port). Its property can be expressed by the response from the in port to out port, which is usually influenced by the frequency. α_1, $L(\omega)$, and α_2 are the responses of the source fiber, medium, and detecting fiber, respectively. In this case they also express the losses. We do not distinguish between the meaning of loss and response strictly in this paper. The coupling loss is included in the loss of the corresponding fi-

1083-3668/2002/$15.00 © 2002 SPIE

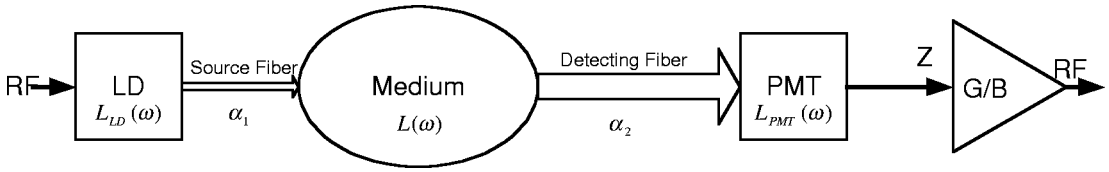

Fig. 1 Transmission model of the rf signal in frequency-domain instruments. The optical link from the LD to the PMT acts as a carrier and adds amplitude and phase information to the rf signal.

ber. Assuming that the power of the LD is P_{LD}, the optical power received by the PMT is P_{PMT}:

$$P_{\mathrm{PMT}}(\omega)=P_{\mathrm{LD}}\alpha_1 L(\omega)\alpha_2. \tag{1}$$

$L_{\mathrm{LD}}(\omega)$ and $L_{\mathrm{PMT}}(\omega)$ are the frequency responses of the optoelectronic components. They are equal to 1 if we use components with enough of a bandwidth. Other parameters in Figure 1 will be explained in the following. The rf signal output by the PMT, expecially its signal to noise ratio (SNR), determines the performance of the instrument.

2.2 Loss of Medium

The loss of medium, $L(\omega)$, is dependent upon its optical properties. We give out its method of calculation based on photon diffusion theory. Generally, we assume that the medium of interest is a uniform, macroscopical, highly scattering medium characterized by an optical absorption coefficient (μ_a), a reduced scattering coefficient (μ_s'), and an average speed of light (c_n). Delivery and detection of light occur on the surface of this ''infinite'' medium half space, which is called semi-infinite geometry. According to the semi-infinite bounding condition, $R(\rho,\omega,\mu_a,\mu_s,c_n)$, the number of photons crossing the medium boundary per unit time per unit area at separation ρ from a unit pencil beam source modulated at frequency $f=\omega/2\pi$, is given by[7,8]

$$R(\rho,\omega,\mu_a,\mu_s',c_n)=\frac{1}{2(2\pi)^{3/2}}\left(\frac{z_0(1+k\rho_0)}{\rho_0^3}\exp(-k\rho_0)+\frac{z_p(1+k\rho_p)}{\rho_p^3}\exp(-k\rho_p)\right), \tag{2}$$

where $z_0=1/\mu_s'$, $z_p=z_0+4D/\kappa$, $D=[3(\mu_a+\mu_s')]^{-1}$, $\kappa\approx 0.426$ for a medium-air boundary, and $\rho_0^2=\rho^2+z_0^2$, $\rho_p^2=\rho^2+z_p^2$, $k=[(\mu_a c_n+i\omega)/Dc_n]^{1/2}$. Note that $R(\rho,\omega,\mu_a,\mu_s',c_n)$ is complex and its amplitude denotes the relative optical intensity to the point source.

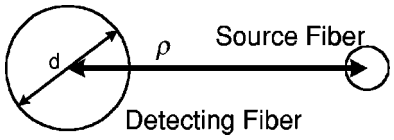

Fig. 2 Delivery and detection of light on the surface of the medium. The source fiber is thought to be a point source. Photons in the detecting area can be collected by the fiber. When d is much smaller than ρ, we assume that the optical power is uniform over the whole detecting area.

The delivery and detection of light on the surface of the medium is shown in Figure 2. The diameter of the detecting fiber is d. Then according to the definition of $R(\rho,\omega,\mu_a,\mu_s',c_n)$, the response (loss) of the medium, $L(\omega)$, can be attained as

$$L(\omega)=\oiint_d \|R(\rho,\omega,\mu_a,\mu_s',c_n)\|dS. \tag{3}$$

For convenience, we assume that the optical power is uniform in the whole detecting area which is close to the intensity at the center of the fiber. The result of this assumption is that the calculated optical power is larger than the real power and it is more applicable when d is much smaller than ρ, which is usually the case in clinical measurements. Then Eq. (3) can be simplified to:

$$L(\omega)=\frac{\pi}{4}d^2\|R(\rho,\omega,\mu_a,\mu_s',c_n)\|. \tag{4}$$

The separation ρ between the source and detecting fibers influences the loss of the medium, which then influences the optical power received by the PMT. Due to the existence of noise, there is a minimal requirement for the optical power received, which limits the maximal separation to get the useful signal.

2.3 Signal, Noise and SNR of the Instrument

In Figure 1, according to the optical detector (PMT), the rf signal received is

$$P_{\text{rf-out}}=\tfrac{1}{2}[mRP_{\mathrm{PMT}}(\omega)g]^2Z=\tfrac{1}{2}[mRP_{\mathrm{LD}}\alpha_1 L(\omega)\alpha_2 g]^2Z, \tag{5}$$

where R is radiant sensitivity (A/W), g is current amplification and Z is the load resistor; the other parameters are those according to Eq. (1). m is the signal modulation index, which is defined as

$$m=\frac{I_0}{I_b-I_{\mathrm{th}}}=\frac{r_{\mathrm{LD}}I_0}{P_{\mathrm{LD}}}, \tag{6}$$

where I_b and I_{th} are the bias current and threshold current of the LD, respectively, r_{LD} is the emitting efficiency (W/A) and I_0 is the signal current, which can be given by Eq. (7) assuming that the resistor of the LD is Z_{LD} and the input signal power is $P_{\text{RF-in}}$:

$$I_0=\sqrt{2P_{\text{rf-in}}/Z_{\mathrm{LD}}}. \tag{7}$$

Substituting Eqs. (6) and (7) into Eq. (5) yields

$$P_{\text{rf-out}} = P_{\text{rf-in}}[r_{\text{LD}} R \alpha_1 L(\omega) \alpha_2 g]^2 \frac{Z}{Z_{\text{LD}}}. \quad (8)$$

From Eq. (8), there is no direct relation between the output power of the LD and the signal intensity received. It is reasonable because the light just acts as a pure carrier. In order to increase the signal received, one can increase the input rf power. Generally the more rf signal can be modulated in the LD with the higher optical power. But it is still subject to the impedance matching of the driver circuits and the safety of the LD.

There are mainly three kinds of noise considered for the instrument: thermal noise (TN), shot noise (SN), and relative intensity noise (RIN). They are related to the average inciting light. Assuming the dc response of the medium is $L(0)$, the average optical power received by the PMT is

$$P_{\text{PMT}} = P_{\text{LD}} \alpha_1 L(0) \alpha_2. \quad (9)$$

Given k is the Boltzmann constant ($1.37e-23$ J/K), T is the kelvin temperature ($\sim$300 K), F is the noise figure of the first amplifier, q is the elementary charge ($1.6e-19C$), I_{dark} is the anode dark current of the PMT, RIN is the intensity noise figure of the LD ($\sim$100 dB/Hz), B is the bandwidth of the instrument and Z is the load resistor ($\sim$50 Ω), we can express the main noises as follows:[15–17]

(i) Thermal noise current density:

$$\langle i_{\text{TN}}^2 \rangle = 4kTF/Z; \quad (10)$$

(i) Shot noise current density:

$$\langle i_{\text{SN}}^2 \rangle = 2q(RP_{\text{PMT}} g^2 + I_{\text{dark}} g); \quad (11)$$

(i) Relative intensity noise current density:

$$\langle i_{\text{RIN}}^2 \rangle = \text{RIN}(RP_{\text{PMT}} g)^2. \quad (12)$$

Then the total noise is

$$P_{\text{noise}} = BZ(\langle i_{\text{TN}}^2 \rangle + \langle i_{\text{SN}}^2 \rangle + \langle i_{\text{RIN}}^2 \rangle). \quad (13)$$

There are still other noise factors which may be divided into these three kinds of noise by modifying the parameters in their expressions. These three kinds of noise present three essential procedures in the transformation from light to electricity: the light itself, the optoelectronic transform and the electronical parts. The shot noise is made up of two parts. Noise coming from dark current behaves differently from general shot noise so in later discussion we exclude it from shot noise and assign it a different name: dark current noise.

From Eqs. (5) and (13), the SNR can be obtained as

$$\text{SNR} = 10 \log(P_{\text{rf-out}} / P_{\text{noise}}). \quad (14)$$

Parameters in Eq. (14) can be calculated by the equations derived earlier. We can then use them to do analyses and simulations for questions concerning FD instruments.

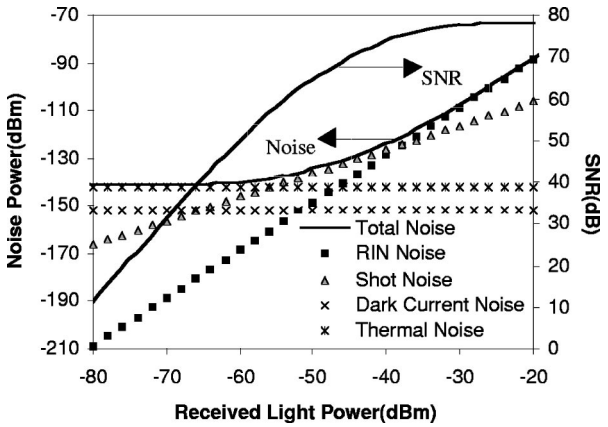

Fig. 3 Noise and SNR properties at different optical powers received: $m=1$, $Z=50\ \Omega$, $B=20$ Hz, and other parameters according to specifications of $R=18$ mA/W at 780 nm, $g=1e4$ at 400 V high voltage (HV), $I_{\text{dark}}=50$ nA, and $F=4.5$ dB. As the inciting optical power increases, the SNR exhibits three stages which correspond to three kinds of noise source.

3 Simulation, Experiment and Analysis

3.1 Noise and SNR Properties with Inciting Optical Power

From that deduced in Sec. 2.3, we can see that both signal and noise are influenced by the optical power received by the PMT. However, noise is related to the average optical power (or dc part of the light) and the signal is determined by the ac part which can be called the ''effective light signal.'' The effective light signal is smaller than the average power due to the frequency response of the loss of the medium. That is to say, cw devices would have better SNRs than FD instruments do. Before we study the performance of the instrument, we first learn the properties of SNR to inciting power because in the final analysis nearly all changes in other parameters can be explained by the change of the optical power received.

The condition for this simulation is that the effective light signal is the same as the average power. We assume this because of the unknown frequency response of the medium. Although it will result in slightly larger signal power than the actual value, it does not influence our understanding about the properties of the SNR. Figure 3 shows the noises and SNR of the system at different optical powers received. The rf signal intensity is always proportional to the optical power. The noise exhibits three stages with an increase of inciting light. When the inciting light is low, thermal noise is the main source and it keeps constant so the SNR increases at the speed of the square of optical power. When the inciting light is increased to a certain value, the shot noise becomes the main source and it is linear to the optical power so the SNR increases linearly. As the inciting light increases to a specific point, the relative intensity noise plays a major role and is linear to the square of the optical power, so SNR saturates. Actually, this kind of change is an intrinsic property of the entire optical detecting system. In NIR applications, generally the light received is very small (attenuation of the medium is about $\sim$100 dB)[12] and the main noise is from shot and thermal sources.

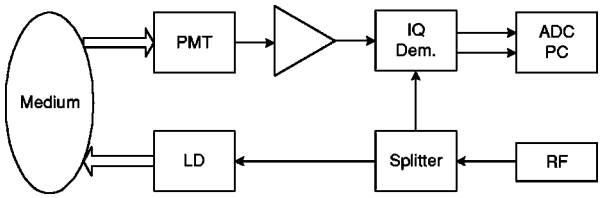

Fig. 4 Experimental setup. This is the general structure of the FD system which is in Fig. 1.

3.2 Separation Experiment and the Maximum Separation

The loss due to propagation in the medium is greatly influenced by the separation. In certain applications, the maximum separation can reflect the performance of the instrument: a larger maximum separation means better sensitivity. In theory, when the SNR decreases to 0 dB because of an increase in separation between the source and detecting fibers, it defines the maximum separation. Signal power and SNR can be measured with satisfactory accuracy at different separations which enables us to check our analysis and calculation.

The experimental setup is shown in Figure 4, included are the LD, Sharp LT024MD, 780 nm; PMT, Hamamatsu, R928; rf source, Wilmanco, 140 MHz. This is a common structure of the FD instrument, which is outlined in Figure 1. The bandwidth of the whole system is about 20 Hz. The test was made on a sample solution with $\mu_a = 0.04$/cm and $\mu_s' = 8$/cm which was made up of intralipid, ink and water. Figures 5(a) and 5(b) show the results and a comparison between the calculated and measured values of the rf signal and its SNR. Considering the error in the parameters' values which will especially bring some differences in absolute values like the rf signal power, we assert that the calculated and measured values were satisfactory, especially the trend of their changing with separation. In Figures 5(a) and 5(b) when the separation was small (less than 3 cm), there was some deviation from calculated values, because the assumption in Sec. 2.2 was not well satisfied at a smaller separation, which means the higher calculated values. When the separation is much larger (say, 8 cm), the values are too small and too difficult to measure exactly, which also brings errors. In the process as the separation decreased, the SNR experienced three stages: a rapid increase, a linear increase, and saturation which corresponded to the three kinds of noise that we analyzed in Sec. 3.1.

Concerning the maximum separation, the criteria of the SNR are used to acquire it. The maximum we measured is about 8.1 cm whose SNR is around 21 dB (Figure 5). Obviously it is smaller than the value of 9.8 cm derived from SNR = 0 dB. In practice, the fact that we can measure the signal means the SNR > 0 dB. So it is necessary to set up a standard for the data acquired by the FD system. We consider this question from two perspectives. Theoretically, the phase detection accuracy of the signal is limited by its SNR. The phase deviation is nearly the inverse of the signal to noise amplitude ratio (SNAR) value when the signal is very weak, which can be written as

$$\Delta P \approx 1/\mathrm{SNAR} = \Delta A/A \ \text{(rad)}, \tag{15}$$

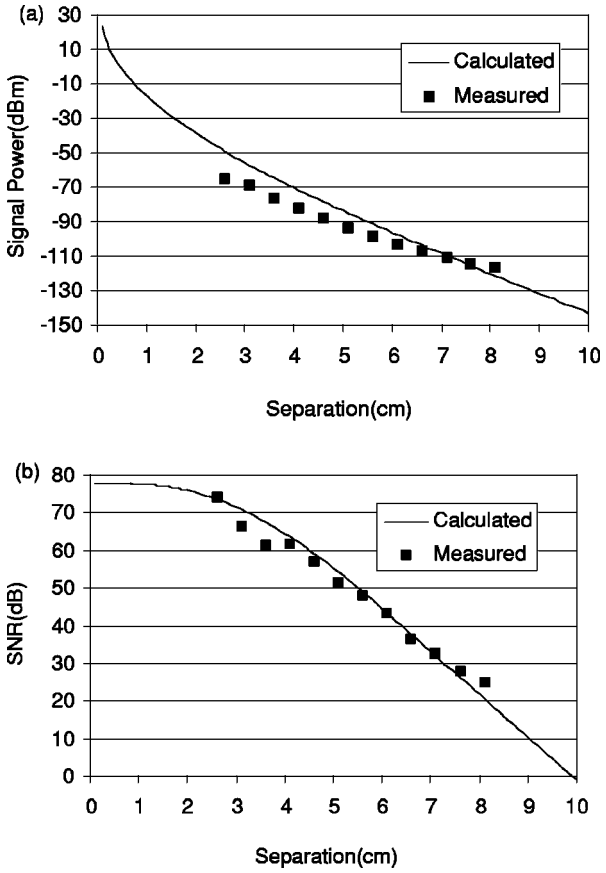

Fig. 5 (a) Signal and (b) SNR comparison: $f = 140$ MHz, $\mu_a = 0.04$/cm, $\mu_s' = 8$/cm, $d = 6$ mm, HV = 400 V, $\alpha_1 P_{\mathrm{LD}} = 4.15$ mW, $\alpha_2 = 0.5$, and other parameters according to Fig. 3. This test was carried out on a sample solution at different separations. Considering the estimation of some parameters, the agreement between calculated and measured values is satisfactory, which is more obvious in the relative values of the SNR.

assuming that ΔP is the phase deviation, ΔA is the noise amplitude and A is the signal amplitude. This means the phase error will be greater than 10° if the SNAR of the signal falls below 5 (Refs. 18 and 19 give similar results). On the other hand, in experiments using lots of tests we also found that the data (both amplitude and phase) are reliable only when the SNAR is about above 5. So we assume that the data are suitable when the amplitude of the signal is five times larger than that of the noise. Then the minimum SNR required is

$$\mathrm{SNR}_{\min} = 20 \log 5 = 14 \ \text{dB}. \tag{16}$$

A factor of 20 is used here in order to be consistent with the definition in Eq. (14). Thus we can get a maximum separation of 8.5 cm from Figure 5(b). Compared to measured values of 8.1 cm, the difference stands at 5%, which is acceptable.

We repeated the test. The calculated and measured values corresponded well with each other and the difference in maximum separation was within 7%. These results show that our model and analysis are valid and they can help us to understand the performance of the instrument and decide whether its quality can satify our requirements in applications.

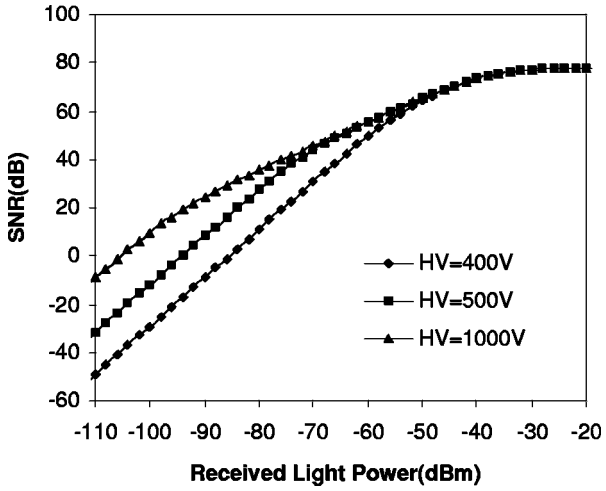

Fig. 6 Influence of high voltage on the SNR: $\rho = 7$ cm, and other parameters according to Fig. 5. Higher voltage gives better SNR performance in the lower inciting light condition which is the normal case in NIR applications.

3.3 Influence of Parameters

The parameters of the instrument which can be changed easily and must be designed to build a machine are current amplification of the PMT, laser power and diameter of the detecting fiber. We can also analyze the choice of these parameters by using the theories in Sec. 2.

3.3.1 *Current Amplification of the PMT*

Current amplification is increased with high voltage applied to the PMT. During the experiments, we generally adjust the high voltage to get a suitable output signal because of possible saturation of the circuit parts. However, it is not appropriate. As we can see from Eqs. (8)–(14) in Sec. 2.3, when the shot noise or RIN noise is the main source of system noise, the SNR would not be influenced by high voltage since the current amplification factor g is canncelled out. However when thermal noise or dark current noise plays a major role, the SNR will increase with applied high voltage, as shown in Figure 6. In the NIR imaging field, the multiply scattered photon signal is very small so we usually replace avalanche photodiode (APD) with the PMT as the optical detector, i.e., the latter condition will usually be met.[12] We then need to set the high voltage as high as it can be in order to make full use of the advantages of the PMT. We can use automatic gain control to eliminate saturation of the electronic parts and get enough of a dynamic range.

When the high voltage increases to a certain degree, dark current noise will exceed thermal noise which means the final sensitivity of the instrument is up to the PMT. The photon-limited SNR can be expressed as

$$\mathrm{SNR} = 10 \log\left\{\frac{[mRP_{\mathrm{PMT}}]^2 g}{4qI_{\mathrm{dark}}B}\right\}. \tag{17}$$

By substituting SNR = 0 dB, we can get the equivalent noise input (ENI) in Eq. (18). It has the same format as the definition of cw light in the PMT manual,[17] which verifies our theoretical model in another way.

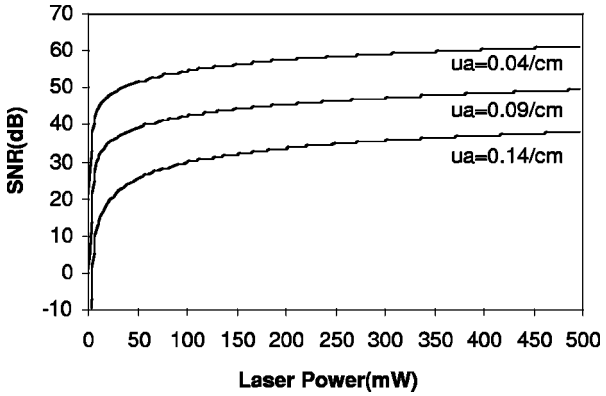

Fig. 7 SNR with different laser powers: $\mu_s' = 8$/cm, $\rho = 7$ cm, and other parameters according to Fig. 5. The optical coefficients and 7 cm separation correspond to the most common clinical usage with penetrating depth of around 3.5 cm. With an increase in LD power, the SNR rapidly increases, linearly increases, and saturates.

$$\mathrm{ENI} = \frac{\sqrt{4qI_{\mathrm{dark}}gB}}{mRg}. \tag{18}$$

3.3.2 *Laser Power*

From Sec. 2.3, we know the rf power received has nothing to do with the output power of the LD directly. The assumption of this analysis is that the modulation index at the different output optical power remains at the same level, which means the higher power LD will correspond to the larger input rf signal. Under this condition it is true that the SNR increases with the laser power as shown in Figure 7. But the increasing speed becomes slower and slower because of the change of the main noise source when the power goes over some specific values. The turning point at which the main noise changes from thermal noise to shot noise can be derived by utilizing Eqs. (10) and (11):

$$P_{\mathrm{PMT1}} = \frac{2kTF}{ZqRg^2}. \tag{19}$$

Below this point the SNR increases rapidly. From Eqs. (11) and (12) the second turning point between shot noise and RIN noise is given by

$$P_{\mathrm{PMT2}} = \frac{2q}{\mathrm{RIN}^* R}. \tag{20}$$

After this point the SNR saturates. Given this information, we should choose the optical power so as to let the inciting light fall into the range given by P_{PMT1} and P_{PMT2} and get the shot-noise-limited SNR.

It also becomes more difficult to couple, sustain a high modulation index and keep the components and patients safe using high power LDs. These enable us to find an optimal laser power in a given application. For instance, for the case with the parameters given in Figure 7 (these optical coefficients and 7 cm separation correspond to the most common clinical usage with penetrating depth around 3.5 cm), ~20 mW laser power corresponds to the first turning point, and the second turning point appears at 450 mW laser power.

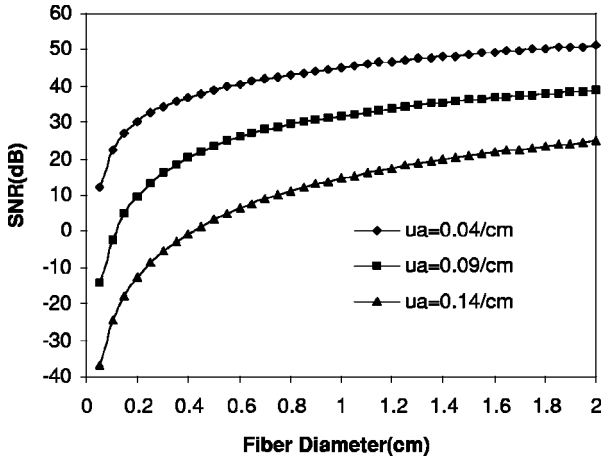

Fig. 8 Influence of the diameter on the SNR: $\mu_s' = 8$/cm, $\rho = 7$ cm, and other parameters according to Fig. 5. The diameter of the detecting fiber should be big enough to satisfy the SNR requirements of the data in a given application.

So the LD should have minimal power of ~20 mW to get a shot-noise-limited SNR. Above this point the SNR increases linearly with the light's power. We need to consider practical operations and find a trade-off between cost and performance. Generally when the laser power is below ~60 mW, which corresponds to ~150 mA bias current, the driver circuits and the modulation have similar complexity (we summarized these from commecial LDs and their specifications). Above this value things become much more complex and power dissipation, temperature control, safety of components and other factors have to be carefully considered and designed. On the other hand, any improvement in performance is very limited by increasing the laser power after this point. For example, by increasing the laser power from 60 to 120 mW, we can get only two times the rise in SNR but the cost of this is far more than twofold. Moreover we definitely get a lower modulation index for 120 mW LDs. So LDs with ~20–~60 mW output power would be a good choice for this application. If we still want to enhance the performance at this stage, we had better consider other factors such as the PMT, filter, etc., which have greater efficiency than light intensity does.

3.3.3 *Diameter of the Detecting Fiber*

In some cases, especially when the object was darker, we found it was impossible to get the signal when the diameter of the detecting fiber was under a certain value. This is easy to understand because there is a minimal requirement for the light received which is proportional to the detecting area. We could not always use big fibers in all applications due to the limitation of dimensions and integration of the heterogeneity.

Theory in Sec. 2 is used to calculate the diameter necessary for the detecting fiber. Figure 8 gives an example in which the SNR changes with the diameter. In this case, in order to sustain the SNR above 0 dB, when $\mu_a = 0.14$/cm, the diameter of the detecting fiber should be at least 5 mm whereas for $\mu_a = 0.09$/cm a fiber diameter of 1 mm is sufficient. Of course we can apply this method to other applications and find the detecting fiber diameter that is suitable.

4 Conclusion

In this paper we presented an analytical method for the performance of FD instruments based on diffusion theory and the transfer properties of optoelectronic components. Because of the simplification and assumption in the model, it will give better results on the properties of instruments. The agreement between experiments and simulations based on this analytical model validates our approach and provides a means by which to optimize the instrument.

The performance of the instrument is influenced by all its parameters. Since the optical detector is key to deciding the sensitivity, the first thing to do is to choose a detector with high radiant sensitivity and current amplification. When we consider the trade-off between the increase of the SNR and the cost there is an optimal laser power. We then choose the detecting fiber with the suitable diameter in order to satisfy the SNR requirement. The performance of the whole instrument could be analyzed by this theoretical model to see whether all the requirements in applications are satisfied.

This method is not limited by diffusion theory or by the semi-infinite bounding condition. It can be applied to other experimental configurations by calculating the loss of the medium using other photon migration theories.

Acknowledgments

The authors would like to thank Chenpeng Mu, Hongyan Ma, and Regine Choe for relevant discussions. They also thank Mary Leonard for text revision. One of the authors (T.T.) acknowledges NIH Grant Nos. CA72895 and CO97065.

References

1. X. Cheng and D. A. Boas, ''Diffuse optical reflection tomography with continuous-wave illumination,'' *Opt. Express* **3**(3), 118–123 (1998).
2. H. Eda et al., ''Multichannel time-resolved optical tomographic imaging system,'' *Rev. Sci. Instrum.* **70**(9), 3595–3602 (1999).
3. V. Ntziachristos, X. Ma, A. G. Yodh, and Britton Chance, ''Multichannel photon counting instrument for spatially resolved near infrared spectroscopy,'' *Rev. Sci. Instrum.* **70**(1), 193–201 (1999).
4. T. O. McBride, B. W. Pogue, S. D. Jiang, U. L. Osterberg, K. D. Paulsen, and S. P. Poplack, ''Initial studies of *in vivo* absorbing and scattering heterogeneity in near-infrared tomographic breast imaging,'' *Opt. Lett.* **26**(11), 822–824 (2001).
5. D. M. Hueber, M. A. Franceschin, H. Y. Ma, Q. Zhang, J. R. Ballesteros, S. Fantini, D. Wallace, V. Ntziachristos, and B. Chance, ''Noninvasive and quatitative near-infrared haemoglobin spectrometry in the piglet brain during hypoxic stress, using a frequency-domain multidistance instrument,'' *Phys. Med. Biol.* **46**, 41–62 (2001).
6. E. M. Sevick, B. Chance, J. Leigh, and M. Maris, ''Quantitation of time- and frequency-resolved optical spectra for the determination of tissue oxygenation,'' *Anal. Biochem.* **195**, 330–351 (1991).
7. B. W. Pogue and M. S. Patterson, ''Error assessment of a wavelength tunable frequency-domain system for noninvasive tissue spectroscopy,'' *J. Biomed. Opt.* **1**(3), 311–323 (1996).
8. J. B. Fishin and E. Gratton, ''Propagation of photon-density waves in strongly scattering media containing an absorbing semi-infinite plane bounded by a straight edge,'' *J. Opt. Soc. Am. A* **10**(1), 127–140 (1993).
9. Y. Yang, H. Liu, X. Li, and B. Chance, ''Low-cost frequency-domain photon migration instrument for tissue spectroscopy, oximetry, and imaging,'' *Opt. Eng.* **36**(5), 1562–1569 (1997).
10. H. Y. Ma, C. W. Du, and B. Chance, ''A homodyne frequency-domain instrument—I&Q phase detection system,'' *Proc. SPIE* **2979**, 826–837 (1997).

11. T. O. McBride, B. W. Pogue, S. Jiang, U. L. Osterberg, and K. D. Paulsen, ''A parallel-detection frequency-domain near-infrared tomography system for hemoglobin imaging of the breast *in vivo*,'' *Rev. Sci. Instrum.* **72**(3), 1817–1824 (2001).
12. B. Chance, M. Cope, E. Gratton, N. Ramaujam, and B. Tromberg, ''Phase measurement of light absorption and scatter in human tissue,'' *Rev. Sci. Instrum.* **69**(10), 3457–3481 (1998).
13. T. H. Pham, O. Coquoz, J. B. Fishkin, E. Anderson, and B. J. Tromberg, ''Broad bandwidth frequency domain instrument for quantitative tissue optical spectroscopy,'' *Rev. Sci. Instrum.* **71**(6), 2500–2513 (2000).
14. S. Feng, F. Zeng, and B. Chance, ''Photon migration in the presence of a single defect: A perturbation analysis,'' *Appl. Opt.* **34**, 3826–3837 (1995).
15. H. Ogawa, ''Microwave and millimeter-wave fiber optic technologies for subcarrier transmission systems,'' *IEICE Trans. Commun.* **e76-b**(9), 1078–1090 (1993).
16. N. Imai, H. Kawamura, T. Imaoka, and E. Ogawa, ''Millimeter wave personal communication system using fiber-optic links,'' *Proc. IEEE MTTS Topical Meetings on Optical Microwave Interactions*, pp. 141–144 (1994).
17. *Photomultiplier Tubes*, revised version, H. Kume, ed., Hamamatsu Photonics K. K., Japan (2000).
18. Y. Chen, C. P. Mu, X. Intes, and B. Chance, ''Signal-to-noise analysis for detection sensitivity of small absorbing heterogeneity in turbid media with single-source and dual-interfering-source,'' *Opt. Express* **9**, 212–224 (2001).
19. Q. Zhang, T. Brukilacchio, T. Gaudett, L. Wang, A. Li, and D. A. Boas, ''Experimental comparison of using continuous-wave and frequency-domain diffuse optical imaging systems to detect heterogeneities,'' *Proc. SPIE* **4250**, 219–238 (2001).